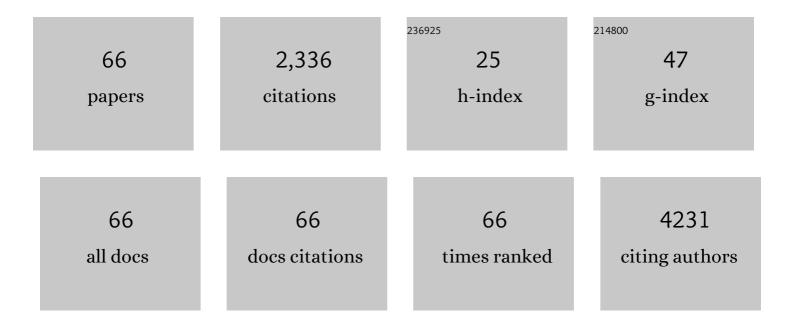
List of Publications by Year in descending order

Source: https://exaly.com/author-pdf/8118159/publications.pdf Version: 2024-02-01



DAMENCLUL

#	Article	IF	CITATIONS
1	Highly accurate diagnosis of lung adenocarcinoma and squamous cell carcinoma tissues by deep learning. Spectrochimica Acta - Part A: Molecular and Biomolecular Spectroscopy, 2022, 265, 120400.	3.9	19
2	Microscopical Quantification of Ionâ€Induced Nanodefects in Monolayer MoS ₂ Based on Differential Reflectance. Advanced Materials Interfaces, 2022, 9, 2101612.	3.7	2
3	Imaging of Defect-Accelerated Energy Transfer in MoS2/hBN/WS2 Heterostructures. ACS Applied Materials & Interfaces, 2022, , .	8.0	1
4	Twist-angle-controlled neutral exciton annihilation in WS ₂ homostructures. Nanoscale, 2022, 14, 5537-5544.	5.6	4
5	Inspection of Line Defects in Transition Metal Dichalcogenides Using a Microscopic Hyperspectral Imaging Technique. Journal of Physical Chemistry Letters, 2022, 13, 2226-2230.	4.6	1
6	In Situâ€Formed Ultralow Wear Tribofilms Induced by Poly(Acrylic Acid)â€ <i>co</i> â€MXeneâ€Modified Polymerâ€Like Carbon Films. Advanced Engineering Materials, 2022, 24, .	3.5	7
7	Defect-Type-Dependent Carrier Lifetimes in Monolayer WS ₂ Films. Journal of Physical Chemistry C, 2022, 126, 4929-4938.	3.1	10
8	High-Precision Intelligent Cancer Diagnosis Method: 2D Raman Figures Combined with Deep Learning. Analytical Chemistry, 2022, 94, 6491-6501.	6.5	18
9	Visualizing ultrafast defectâ€controlled interlayer electronâ€phonon coupling in van der Waals heterostructures. Advanced Materials, 2022, , 2106955.	21.0	1
10	Self-Poisoning by C ₂ Products in CO ₂ Photoreduction Using a Phosphorus-Doped Carbon Nitride with Nitrogen Vacancies. ACS Sustainable Chemistry and Engineering, 2022, 10, 5758-5769.	6.7	14
11	Friction-Induced Clustered Rearrangement at a PbS Quantum Dot Nanocoating via Long-Term Lubrication under an Atmosphere Environment. Journal of Physical Chemistry Letters, 2022, 13, 6342-6348.	4.6	1
12	Energy dissipation through phonon and electron behaviors of superlubricity in 2D materials. , 2021, , 145-166.		0
13	Rapid thin-layer WS2 detection based on monochromatic illumination photographs. Nano Research, 2021, 14, 840-845.	10.4	8
14	High-performance SERS substrate based on perovskite quantum dot–graphene/nano-Au composites for ultrasensitive detection of rhodamine 6G and <i>p</i> -nitrophenol. Journal of Materials Chemistry C, 2021, 9, 9011-9020.	5.5	18
15	Accurate diagnosis of lung tissues for 2D Raman spectrogram by deep learning based on short-time Fourier transform. Analytica Chimica Acta, 2021, 1179, 338821.	5.4	23
16	A new opportunity for the emerging tellurium semiconductor: making resistive switching devices. Nature Communications, 2021, 12, 6081.	12.8	25
17	Raman spectroscopy as a potential diagnostic tool to analyse biochemical alterations in lung cancer. Analyst, The, 2020, 145, 385-392.	3.5	30
18	Ultrasensitive SERS detection of rhodamine 6G and p-nitrophenol based on electrochemically roughened nano-Au film. Talanta, 2020, 210, 120631.	5.5	62

#	Article	IF	CITATIONS
19	Direct Visualization of Exciton Transport in Defective Few‣ayer WS ₂ by Ultrafast Microscopy. Advanced Materials, 2020, 32, e1906540.	21.0	50
20	Tunable Exciton Radiative Recombination Lifetime in Twisted Bilayer Molybdenum Disulfide. Journal of Physical Chemistry C, 2020, 124, 21123-21128.	3.1	8
21	Band Structure, Band Offsets, and Intrinsic Defect Properties of Few-Layer Arsenic and Antimony. Journal of Physical Chemistry C, 2020, 124, 7441-7448.	3.1	9
22	Influence of elastic property on the friction between atomic force microscope tips and 2D materials. Nanotechnology, 2020, 31, 285710.	2.6	14
23	Layer-dependent signatures for exciton dynamics in monolayer and multilayer WSe2 revealed by fluorescence lifetime imaging measurement. Nano Research, 2020, 13, 661-666.	10.4	12
24	Exploring interlayer interaction of SnSe2 by low-frequency Raman spectroscopy. Physica E: Low-Dimensional Systems and Nanostructures, 2019, 105, 7-12.	2.7	8
25	Controllable Interlayer Charge and Energy Transfer in Perovskite Quantum Dots/ Transition Metal Dichalcogenide Heterostructures. Advanced Materials Interfaces, 2019, 6, 1901263.	3.7	17
26	Fourier transform infrared and Ramanâ€based biochemical profiling of different grades of pure foetalâ€ŧype hepatoblastoma. Journal of Biophotonics, 2019, 12, e201800304.	2.3	4
27	Exciton Radiative Recombination Dynamics and Nonradiative Energy Transfer in Two-Dimensional Transition-Metal Dichalcogenides. Journal of Physical Chemistry C, 2019, 123, 10087-10093.	3.1	31
28	Neutral and defect-induced exciton annihilation in defective monolayer WS ₂ . Nanoscale, 2019, 11, 7913-7920.	5.6	36
29	Insertion of an ultrathin Al ₂ O ₃ interfacial layer for Schottky barrier height reduction in WS ₂ field-effect transistors. Nanoscale, 2019, 11, 4811-4821.	5.6	24
30	Reduced Binding Energy and Layer-Dependent Exciton Dynamics in Monolayer and Multilayer WS ₂ . ACS Nano, 2019, 13, 14416-14425.	14.6	17
31	Interlayer interaction on twisted interface in incommensurate stacking MoS2: A Raman spectroscopy study. Journal of Colloid and Interface Science, 2019, 538, 159-164.	9.4	15
32	Asymmetric Modulation on Exchange Field in a Graphene/BiFeO3 Heterostructure by External Magnetic Field. Nano Letters, 2018, 18, 2435-2441.	9.1	22
33	Improvement on thermal stability of TiAlSiN coatings deposited by IBAD. Surface Engineering, 2018, 34, 504-510.	2.2	8
34	Layer-Number-Dependent Exciton Recombination Behaviors of MoS ₂ Determined by Fluorescence-Lifetime Imaging Microscopy. Journal of Physical Chemistry C, 2018, 122, 18651-18658.	3.1	21
35	Fabrication of in situ carbon fiber/aluminum composites via friction stir processing: Evaluation of microstructural, mechanical and tribological behaviors. Composites Part B: Engineering, 2018, 139, 97-105.	12.0	81
36	Electrochemical functionalization of 316 stainless steel with polyaniline-graphene oxide: Corrosion resistance study. Materials Chemistry and Physics, 2017, 198, 90-98.	4.0	54

#	Article	IF	CITATIONS
37	Thickness dependent friction on few-layer MoS ₂ , WS ₂ , and WSe ₂ . Nanotechnology, 2017, 28, 245703.	2.6	41
38	Corrosion resistance and micro-tribological properties of nickel hydroxide-graphene oxide composite coating. Diamond and Related Materials, 2017, 76, 150-156.	3.9	35
39	Superlubricity of a graphene/MoS ₂ heterostructure: a combined experimental and DFT study. Nanoscale, 2017, 9, 10846-10853.	5.6	133
40	Magnetic proximity effect in graphene coupled to a <mml:math xmlns:mml="http://www.w3.org/1998/Math/MathML"><mml:mrow><mml:mi>BiFe</mml:mi><mml:msub><mml: mathvariant="normal">O<mml:mn>3</mml:mn></mml: </mml:msub></mml:mrow> nanoplate. Physical Review B, 2017, 95, .</mml:math 	mi 3.2	57
41	Au-Modified Monolayer MoS ₂ Sensor for DNA Detection. Journal of Physical Chemistry C, 2016, 120, 11204-11209.	3.1	67
42	Strain-Gradient Modulated Exciton Emission in Bent ZnO Wires Probed by Cathodoluminescence. ACS Nano, 2016, 10, 11469-11474.	14.6	11
43	Growth of high quality, high density single-walled carbon nanotube forests on copper foils. Carbon, 2016, 98, 624-632.	10.3	31
44	Microstructure and mechanical properties of TiAlSiN nano-composite coatings deposited by ion beam assisted deposition. Science China Technological Sciences, 2015, 58, 1682-1688.	4.0	9
45	Enhancing the interlayer adhesive force in twisted multilayer MoS ₂ by thermal annealing treatment. Nanotechnology, 2015, 26, 405708.	2.6	21
46	Lateral graphene p–n junctions formed by the graphene/MoS ₂ hybrid interface. Nanoscale, 2015, 7, 11611-11619.	5.6	53
47	Chalcogen vacancies in monolayer transition metal dichalcogenides and Fermi level pinning at contacts. Applied Physics Letters, 2015, 106, .	3.3	151
48	3D Behavior of Schottky Barriers of 2D Transition-Metal Dichalcogenides. ACS Applied Materials & Interfaces, 2015, 7, 25709-25715.	8.0	134
49	Fabrication of micro grooves on silicon by micro optical fiber enhanced pulse laser irradiation. Journal of Micromechanics and Microengineering, 2015, 25, 075021.	2.6	0
50	Step-by-Step Fracture of Two-Layer Stacked Graphene Membranes. ACS Nano, 2014, 8, 10246-10251.	14.6	34
51	Laser wavelength effects on (Ti, Al, Si)N in near-field laser nanostructuring by micron optical fiber enhanced irradiation. Science China Technological Sciences, 2013, 56, 3012-3016.	4.0	0
52	First-principles calculations of the electronic structure and defects of Al2O3. Journal of Applied Physics, 2013, 114, .	2.5	28
53	Flower-like and hollow sphere-like ZnO assisted by microorganisms and their UV absorption and photo catalytic performance. Journal of Materials Science: Materials in Electronics, 2013, 24, 36-43.	2.2	11
54	Solvatochromic Effect on the Photoluminescence of MoS ₂ Monolayers. Small, 2013, 9, 1312-1315.	10.0	131

#	Article	IF	CITATIONS
55	Sulfur vacancies in monolayer MoS2 and its electrical contacts. Applied Physics Letters, 2013, 103, .	3.3	327
56	Laser induced twin-groove surface texturing based on optical fiber modulation. Laser Physics, 2013, 23, 056005.	1.2	0
57	Laser etching of groove structures with micro-optical fiber-enhanced irradiation. Nanoscale Research Letters, 2012, 7, 318.	5.7	3
58	FDTD simulation on laser-induced enhancement of electric field in the near-field apertureless probe system. Laser Physics Letters, 2012, 9, 511-518.	1.4	2
59	Oxygen vacancy levels and electron transport in Al2O3. Applied Physics Letters, 2010, 96, 032905.	3.3	119
60	Electronic and atomic structure of metal- <mml:math xmlns:mml="http://www.w3.org/1998/Math/MathML" display="inline"><mml:mrow><mml:msub><mml:mrow><mml:mtext>HfO</mml:mtext></mml:mrow><mml:mn> Physical Review B, 2010, 81, .</mml:mn></mml:msub></mml:mrow></mml:math 	23/2mml:n	າກ ²³ /mml:m
61	Passivation of oxygen vacancy states and suppression of Fermi pinning in HfO2 by La addition. Applied Physics Letters, 2009, 94, .	3.3	51
62	Oxygen vacancy levels and interfaces of Al2O3. Microelectronic Engineering, 2009, 86, 1668-1671.	2.4	40
63	Te-induced modulation of the Moâ^•HfO2 interface effective work function. Applied Physics Letters, 2008, 92, .	3.3	13
64	p -type Fermi level pinning at a Si:Al2O3 model interface. Applied Physics Letters, 2008, 93, .	3.3	28
65	Electronic structure and defects of high dielectric constant gate oxide La2Hf2O7. Applied Physics Letters, 2007, 90, 062901.	3.3	26
66	Oxygen vacancies in high-k oxides. Microelectronic Engineering, 2007, 84, 2028-2031.	2.4	82